ELASTIC BEHAVIOR OF ZEOLITE BOGGSITE IN SILICON OIL AND AQUEOUS MEDIUM: A CASE OF HP-INDUCED OVER-HYDRATION

American Mineralogist, Volume 95, pages 1247–1256, 2010

Elastic behavior of zeolite boggsite in silicon oil and aqueous medium: A case of high-pressure-induced over-hydration

Rossella Arletti,[1,*] Simona Quartieri,[2] and Giovanna Vezzalini[1]

[1]Dipartimento di Scienze della Terra, Università di Modena e Reggio Emilia, Via S. Eufemia 19, 41100 Modena, Italy
[2]Dipartimento di Scienze della Terra, Università di Messina, Viale Ferdinando Stagno d'Alcontres 31, 98166 Messina S. Agata, Italy

Abstract

This paper reports the results of an in situ high-pressure synchrotron X-ray powder diffraction investigation on the natural zeolite boggsite [$(K_{0.06}Na_{0.36}Sr_{0.01}Ca_{7.00}Mg_{1.20})(Al_{17.52}Si_{78.62}Fe_{0.05}O_{192})\cdot 82.3\ H_2O$]. The study was performed using both a (16:3:1) methanol:ethanol:water mixture (m.e.w.) as a nominally "penetrating" hydrostatic *P*-transmitting medium and silicon oil (s.o.) as a "non-penetrating" medium. The studied pressure ranges are: P_{amb}–7.6 and P_{amb}–5.9 GPa in m.e.w and s.o., respectively. No complete X-ray amorphization is observed up to the highest investigated pressures, and the original unit-cell parameters are almost completely recovered upon decompression in both media. The reductions of *a*, *b*, *c*, and *V*, within the pressure-ranges investigated, are 5.3, 4.2, 4.0, and 13.0% in s.o. and 4.1, 4.1, 3.8, and 11.5% in m.e.w. The Rietveld structural refinements of the powder patterns of the experiments in m.e.w. converged successfully up to 3.6 GPa and demonstrated the penetration of 13 additional water molecules between 0.3 and 2.9 GPa. This over-hydration occurs without any unit-cell volume expansion and can be explained by the fact that no new extraframework sites arise during compression and that water penetration is the only factor to increase the occupancy of already existing sites. Boggsite compressibility is higher in s.o. than in m.e.w. In particular, compressibility in m.e.w. is lower below 3 GPa, whereas above this pressure, the *P*-*V* trend becomes similar in the two media. This can be ascribed to the fact that, during water molecule penetration ($0.3 < P < 3$ GPa), the effect of the *P*-transmitting medium is directed to compress the system as well as to penetrate the channels.

Keywords: Zeolite, boggsite, high pressure, compressibility, over-hydration, crystal structure, synchrotron XRPD data

Introduction

Zeolites represent the fruitful symbiosis among mineralogists, crystal chemists, industrial scientists and engineers. Zeolites are used in absorption processes, ion-exchange, molecular sieving, and catalysis (Bish and Carey 2001; Corma 1997). The behavior of both natural and synthetic zeolite materials under high temperature (HT) (Alberti and Martucci 2005; Bish and Carey 2001; Cruciani 2006) or high pressure (HP) has been extensively investigated, due to the impact of these thermodynamic parameters on their structure, stability and, consequently, applications.

High-pressure studies on zeolites to date used either "pore penetrating" [usually aqueous-alcohol mixtures; see Ori et al. (2008) for a review] or "non-penetrating" *P*-transmitting media [usually silicon oil (see, i.e., Leardini et al. 2010) or glycerol (see, i.e., Gatta 2008)]. The former media are involved in the so-called pressure-induced hydration (PIH) phenomenon (Lee et al. 2004), which is characterized by the penetration of additional water molecules into the zeolite channels. On the basis of these experiments, it was concluded that zeolites can experience different effects: (1) HP-induced structural modifications, without over-hydration; (2) PIH based on increasing occupancy of already existing water sites; and/or (3) PIH accompanied by the onset of new water sites (see Ori et al. 2008 for a review). Over-hydration and consequent structural modifications can, in principle, significantly modify zeolite properties, opening possible new scenarios for their industrial applications.

In parallel, a relevant number of HP studies have been performed on zeolites with "non-penetrating" media, often based on a combined experimental-computational approach (see Fois et al. 2008 for a review). From these investigations, the crucial role of the extraframework content on the zeolite response—in terms of deformation mechanisms and compressibility values—emerged clearly (Fois et al. 2004; Gatta 2008).

In this work we report the results of a HP study performed on boggsite [IZA code BOG, Baerlocher et al. (2001)], a rare natural zeolite with a fascinating topology. Boggsite was discovered in Eocene basalts near Goble (Columbia County, Oregon) and first described by Howard et al. (1990). A second occurrence of this mineral was described (Galli et al. 1995; Alberti et al. 2001) from the Jurassic Ferrar dolerites of Mt. Adamson (Northern Victoria Land, Antarctica).

The crystal structure of boggsite was solved by Pluth and Smith (1990) on a crystal from Goble. The framework (topology and space group *Imma*) has been described by the interconnection of polyhedral subunits 4^25^4, 4^26^4, 5^46^2 (found also in terranovaite), 5^26^2 (present with 5^46^2 in gottardiite), and 4^26^2. A straight 12-membered ring channel runs along [100], and a straight 10-membered ring channel develops in the [010] direction (Figs. 1a and 1b). These channels are connected by 10-membered ring windows. Boggsite is characterized by strong disorder in both

* E-mail: rossella.arletti@unimore.it

cation and H_2O molecule distribution, with many partially occupied sites weakly interacting with the extraframework population (Pluth and Smith 1990; Zanardi et al. 2004).

The chemical formulae of boggsite from Goble and Mt. Adamson (Table 1) indicate a constant Si/Al ratio (ca. 4.3). This is a common value for the already known pentasil zeolites, but low when compared with that of the other pentasil zeolites from Mt. Adamson (Alberti et al. 2001). Calcium is always the most abundant extraframework cation, whereas Na is variable and can reach contents nearly equal to that of calcium. Minor quantities of K and Mg are present.

The linear development and dimensions of boggsite channels make this topology potentially suitable for industrial and environmental applications. Whereas some patents report the use of synthetic boggsite as a catalyst, in which molecular dynamics calculations were used to simulate anisotropic molecular diffusion phenomena in boggsite (Clark et al. 2000; Sanborn et al. 2001), a hydrothermal synthesis of boggsite was used by ChePa and Baharun (2005).

Structural modifications under non-ambient conditions play an important role in assessing the suitability of a zeolite structure for technological applications. The applicative potentialities of boggsite suggested to investigate its behavior and stability under HT conditions, following the dehydration and rehydration processes (Zanardi et al. 2004). This work demonstrated that boggsite is characterized by an extremely rigid structure, with a cell-volume contraction of less than 1.4% (up to 500 °C), one of the lowest found for natural zeolites. Moreover, the HT structure of boggsite is capable of holding Ca cations in fourfold coordination, a feature often considered as a potential for structure collapse.

The HP behavior of this microporous material has not been investigated to date. The specific aims of this study are: (1) to investigate the elastic behavior and the HP-structural evolution of boggsite by means of in situ synchrotron X-ray powder diffraction (XRPD), using both "penetrating" and "non-penetrating"

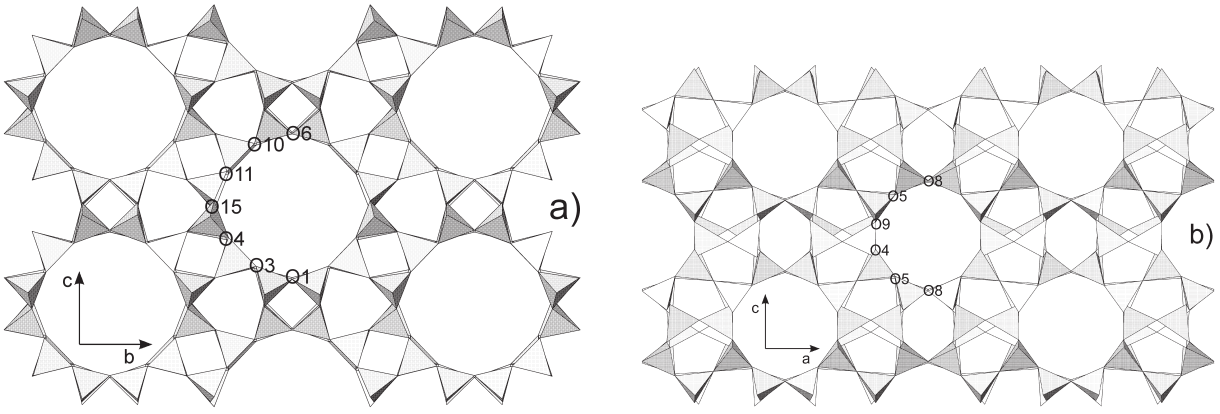

FIGURE 1. The boggsite framework viewed down [100] (**a**) and [010] (**b**) directions, showing the 12- and 10-membered ring channels, respectively.

TABLE 1. Crystal-chemical data reported for boggsite specimens from different localities

Occurrence locality	XRD method	*a* (Å)	*b* (Å)	*c* (Å)	*V* (Å³)	Chemical composition from EMPA	Total extraframework electron number from refinement
Goble (Howard et al. 1990)	powder	20.21(2)	23.77(2)	12.80(1)	6149.0	$[K_{0.16}Na_{2.94}Ca_{7.77}Mg_{0.13}]$ $[Al_{18.29}Si_{77.61}Fe_{0.10}O_{192}]\cdot 70\ H_2O$ Si/Al = 4.2 Cations: 192 electrons Water molecules: 700 electrons	
Goble (Pluth and Smith 1990)	single crystal	20.236(2)	23.798(1)	12.798(1)	6163.2	Howard et al. (1990)	1096
Mt. Adamson (Galli et al.1995)	Gandolfi camera	20.25(2)	23.82(1)	12.78(1)	6164.5	$[K_{1.05}Na_{4.97}Sr_{0.04}Ca_{5.43}Mg_{0.33}Ba_{0.04}]$ $[Al_{18.49}Si_{77.62}Fe_{0.14}O_{192}]\cdot 70\ H_2O$ Si/Al = 4.2 Cations: 191 electrons Water molecules: 700 electrons	
Mt. Adamson (Zanardi et al. 2004)	single crystal	20.291(1)	23.840(1)	12.807(1)	6195.2	$[K_{0.06}Na_{0.36}Sr_{0.01}Ca_{7.00}Mg_{1.20}]$ $[Al_{17.52}Si_{78.62}Fe_{0.05}O_{192}]\cdot 70\ H_2O$ Si/Al = 4.5 Cations: 160 electrons Water molecules: 700 electrons	407
Mt. Adamson (this work)	powder	20.3266(6)	23.876(8)	12.8252(5)	6224.3	$[K_{0.06}Na_{0.36}Sr_{0.01}Ca_{7.00}Mg_{1.20}]$ $[Al_{17.52}Si_{78.62}Fe_{0.05}O_{192}]\cdot 82.3\ H_2O$ Si/Al = 4.5 Cations: 160 electrons Water molecules: 823 electrons	955

P-transmitting media; (2) to verify the capacity of boggsite to host additional water molecules among the numerous partially occupied extraframework sites present in its structure; (3) to single out the influence of different media on the compressibility and HP deformation mechanisms of boggsite; and (4) to compare the elastic and thermal behaviors of boggsite.

Experimental methods and data analysis

Although only two occurrences have been reported in the literature, the unit-cell parameters and the chemical compositions of different boggsite specimens (Howard et al. 1990; Pluth and Smith 1990; Galli et al. 1995; Zanardi et al. 2004) reveal considerable variability (Table 1). The sample used for this study was obtained from the same specimen used by Zanardi et al. (2004) from Mt. Adamson, Northern Terra Victoria Land (Antarctica). Zanardi et al. (2004) did not measure the water content of Mt. Adamson boggsite. We determined the water content by thermogravimetric analysis on a 2 mg sample using a Seiko SSC/5200 instrument, operating at 20 °C/min from 25 to 900 °C in air. The determined weight loss is 19.60%, corresponding to 82.3 water molecules (Table 1).

Synchrotron X-ray powder diffraction experiments and data analysis

The HP synchrotron XRPD experiments were performed at the SNBL1 (BM01a) beamline at the European Synchrotron Radiation Facility (ESRF), using modified Merril-Bassett DACs (Miletich et al. 2000). To test the HP behavior of boggsite with both "penetrating" and "non-penetrating" media, two different experiments were performed, using a (16:3:1) mixture of methanol:ethanol:water (m.e.w.) and silicon oil (s.o.), respectively. Moreover, since no XRPD structural refinements on boggsite at ambient conditions were available in the literature, we performed a data collection at room pressure, to obtain the unit-cell parameters and the starting structural model to be used in the analysis of the data collected under HP.

Ambient-pressure experiment. The P_{amb} XRPD experiment was performed at the BM08 beamline at ESRF (Grenoble) in the Debye-Sherrer geometry. The sample was placed in a quartz capillary mounted on a goniometric spinning head and the diffraction pattern was collected with fixed wavelength of 0.7293 Å on an image plate placed at 288.47 mm from the sample. The Rietveld profile fitting was performed in the 2θ range 2.5–45.5° using the GSAS package (Larson and Von Dreele 1996), with the EXPGUI (Toby 2001) interface (Fig. 2a). The structure reported by Zanardi et al. (2004) was used as the starting model for the refinement. The background curve was fitted by a Chebyshew polynomial with an average of 24 coefficients. The pseudo-Voigt profile function proposed by Thomson et al. (1987) and cut-off of the peak intensity were applied. The following refinement strategy was used for P_{amb} and HP structural refinements. (1) The scale factor, the zero-shift, and the unit-cell parameters were allowed to vary for all refinement cycles. (2) Following the initial refinement cycles, the refined structural parameters for each data histogram obtained include: fractional coordinates for all atoms {soft-restraints were applied to the T-O distances [Si-O = 1.60(2)–1.63(2)]}. The weight was gradually decreased after the initial stages of refinement, up to a final weight = 10; occupancy factors for extraframework sites and thermal isotropic displacement factors for all atoms (the isotropic displacement parameters were constrained by using the same value for all tetrahedral cations, a second value for all framework O atoms, and a third one for all the extraframework sites). (3) Occupancy factors and isotropic thermal displacement factors for extraframework sites were varied in alternate cycles. As a result of the Rietveld refinement, the same extraframework sites found by Zanardi et al. (2004) were located, even if with different occupancy factors. The total electron number obtained for the extraframework species was 955.

HP experiments. Table 2 reports the experimental parameters relative to the measurements performed as a function of pressure in s.o. and m.e.w. Pressure was calibrated using the ruby fluorescence method (Forman et al. 1972) on the non-linear hydrostatic pressure scale (Mao et al. 1986). The estimated precision in the pressure values is 0.1 GPa. The sample was rocked by ±2° in φ to reduce texture in the diffraction images. The experiments in s.o. were performed from 0.1 to 9.3 GPa, whereas those in m.e.w. were performed from 0.3 to 7.6 GPa. Other patterns were collected upon decompression, from the highest pressure to P_{amb}. One-dimensional diffraction patterns were obtained by integrating the two dimensional images with the program FIT2D (Hammersley et al. 1996). Selected integrated patterns are reported in Figures 2b and 2c, for s.o. and m.e.w., respectively.

Rietveld profile fittings to obtain the unit-cell parameters were performed using the GSAS package (Larson and Von Dreele 1996) with the EXPGUI (Toby 2001) interface, up to 5.9 GPa in s.o. (the quality of the higher pressure patterns were too low for the refinement), and up to 7.6 GPa in m.e.w. The starting atomic coordinates were obtained from the structural model determined by the P_{amb} experiment. The background curves were fitted by a Chebyshev polynomial (Table 2). The pseudo-Voigt profile function proposed by Thomson et al. (1987) and cut-off of the peak intensity were applied. The refined cell parameters as a function of pressure are reported in Table 3 and Figures 3a and 3b, for s.o. and m.e.w., respectively.

The quality of the data collected in m.e.w. allowed for complete structural refinements up to 3.6 GPa. The refinement strategy used for the P_{amb} experiment was applied to the structural refinement of boggsite compressed in m.e.w. Table 4 reports the details of the four selected structural refinements at P_{amb}, 2.5 GPa, 3.6 GPa, and P_{amb}(rev) discussed below.

The isothermal bulk moduli of boggsite compressed in s.o. and m.e.w. were determined with the EOS-FIT program (Angel 2001), using a truncated second-order Birch-Murnaghan equation of state (Birch 1974).

Results and discussion

Inspection of Figure 2 indicates that, for both *P*-transmitting media, the peak intensities decrease and the peak profiles become broader with increasing pressure. These effects are particularly evident in the patterns collected in s.o. and can be due to several factors, such as an increase in the long-range structural disorder, and the presence of texture effects. However, both HP data sets demonstrate that boggsite does not undergo complete amorphization up to the highest investigated pressure.

Elastic behavior in silicon oil

Although boggsite in s.o. was compressed to 9.3 GPa, the unit-cell parameters were successfully refined only to 5.9 GPa. In this *P* range, a unit-cell volume reduction of 13.0% was observed. The unit-cell parameters undergo an isotropic decrease up to about 1 GPa followed by anisotropic behavior above this pressure. In the whole range P_{amb}–5.9 GPa, the unit-cell axes reductions are 5.3, 4.2, and 4.0% for *a*, *b*, and *c*, respectively (Table 3; Fig. 3a).

The unit-cell parameters of the P_{amb} pattern are completely recovered upon decompression, but a hysteresis effect is observed at 4.2 GPa(rev). This effect completely disappears at P_{amb}(rev) (Fig. 3a; Table 3). On the other hand, the P_{amb} peak intensities are only partially recovered (Fig. 2b). The hysteresis effect could be

Table 2. Experimental and structural refinement parameters for the XRPD measurements in silicon oil (s.o.) and (16:3:1) methanol:ethanol:water (m.e.w.)

	s.o.	m.e.w.
λ	0.7355	0.70026
Detector	MAR345 (pixel dimension = 150 μm)	MAR345 (pixel dimension = 150 μm)
Sample-detector distance (mm)	230	221
Exposure time (s)	600	180
P-range (GPa)	0.1–9.3	0.3–7.6
Δ*P* increment (GPa)	0.3–0.7	0.2–0.7
Sample equilibration time (min)	30	30
Integration 2θ range of the powder patterns (°)	0–35.5	0–37
No. of coefficients used in the Chebyshev polynomial	22	25

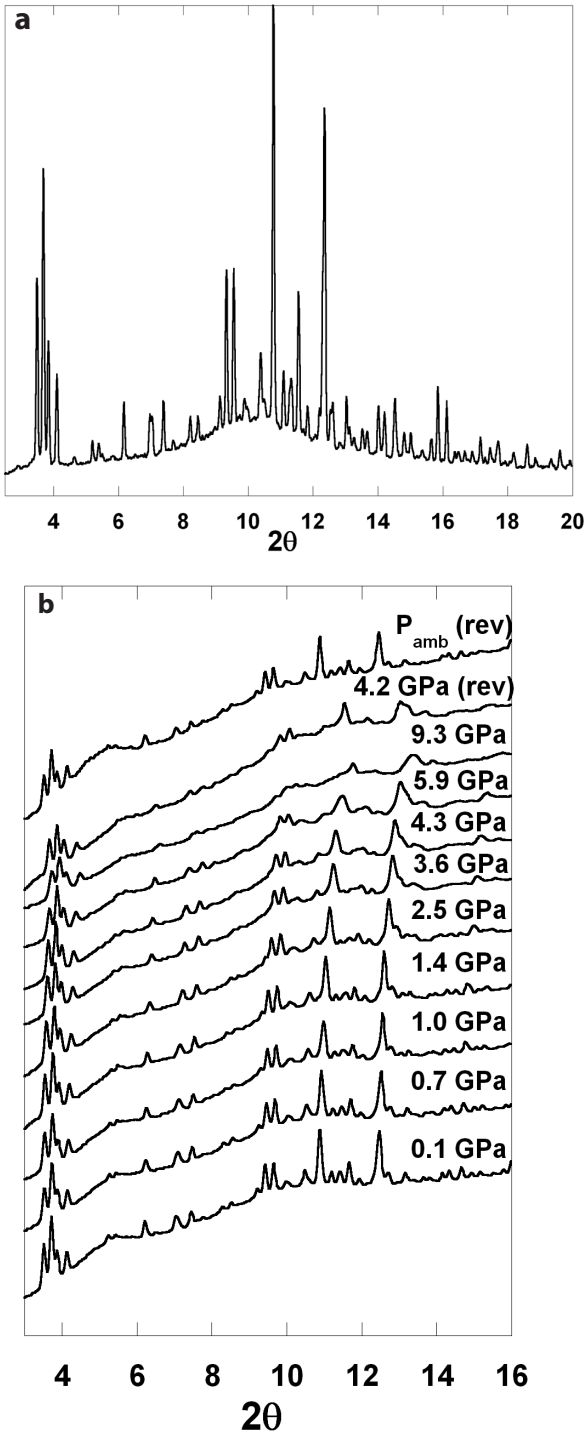

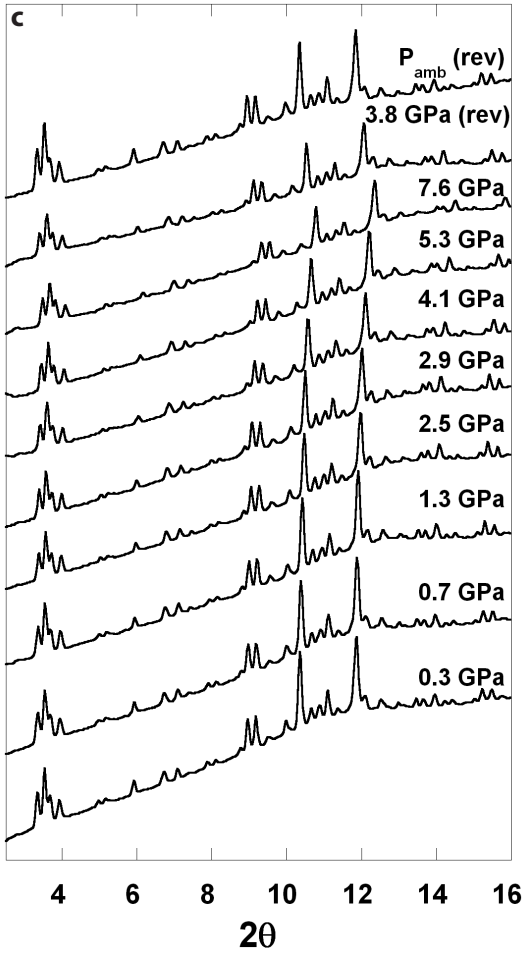

FIGURE 2. (**a**) Boggsite XRPD pattern collected at P_{amb} conditions. (**b** and **c**) selected integrated powder patterns, collected in silicon oil and (16:3:1) methanol:ethanol:water, respectively, reported as a function of pressure. The patterns at the top of the figures (rev) were collected during decompression.

due to the strong compression of the sample during the experiment up to 9.3 GPa and short equilibration time.

The elastic parameters, obtained using the data weighted by the uncertainties in P and V, are $V_0 = 6240(6)$ Å^3, $K_0 = 31.1(4)$ GPa. Since the bulk modulus values determined for zeolites with "non-penetrating" P-transmitting media range from 21 to 72 GPa (Leardini et al. 2010), boggsite can be classified as one of the most compressible zeolites.

Elastic behavior in (16:3:1) methanol:ethanol:water

From P_{amb} to 7.6 GPa, a unit-cell volume reduction of about 11.5% was observed for boggsite compressed in m.e.w, whereas the unit-cell axes undergo an almost isotropic reduction ($\Delta a = \Delta b = 4.1$, $\Delta c = 3.8\%$). Contrary to observations in s.o., the structural deformations induced by HP recover without any hysteresis effect (Figs. 2c and 3b; Table 3).

A discontinuity between 2.5 and 2.9 GPa is evident in the P-cell parameters shown in Figure 3b. The elastic parameters calculated between 2.9 and 7.6 GPa using the data weighted by the uncertainties in P and V, are: $V_0 = 6405(17)$ Å^3, $K_0 = 37(1)$ GPa. Elastic parameters were not calculated for the first P-range because in this pressure regime a variation in the extraframework composition of the system is observed, due to the penetration of additional water molecules (see below). As in s.o., compressibility in m.e.w. is high when compared to other natural and synthetic zeolites studied with "penetrating" aqueous media (Ori et al. 2008).

TABLE 3. Unit-cell parameters of boggsite at the investigated pressures, using silicon oil (s.o.) and (16:3:1) methanol:ethanol:water (m.e.w.)

P (GPa)	a (Å)	b (Å)	c (Å)	V (Å^3)
		s.o.		
P_{amb}	20.3266(6)	23.8760(8)	12.8252(5)	6224.3(4)
0.1	20.305(1)	23.837(1)	12.819(1)	6205(1)
0.4	20.253(1)	23.775(2)	12.788(1)	6158(1)
0.7	20.220(2)	23.737(2)	12.768(2)	6128(1)
1.1	20.119(2)	23.681(3)	12.709(3)	6055(2)
1.4	20.019(3)	23.635(4)	12.660(2)	5990(2)
1.9	19.899(3)	23.513(5)	12.599(3)	5895(2)
2.5	19.799(4)	23.391(6)	12.546(4)	5810(3)
3.0	19.722(5)	23.326(7)	12.513(5)	5756(4)
3.6	19.629(6)	23.211(8)	12.467(6)	5680(4)
4.3	19.511(7)	23.100(9)	12.412(7)	5594(5)
5.3	19.308(9)	22.96(1)	12.331(9)	5467(6)
5.9	19.24(1)	22.87(1)	12.31(1)	5415(7)
4.2(rev)	19.11(1)	22.86(2)	12.28(1)	5365(10)
P_{amb}(rev)	20.303(2)	23.833(2)	12.827(2)	6207(1)
		m.e.w.		
P_{amb}	20.3266(6)	23.8760(8)	12.8252(5)	6224.3(4)
0.3	20.299(1)	23.854(1)	12.8164(9)	6205.9(9)
0.5	20.284(1)	23.837(1)	12.809(1)	6193(9)
0.7	20.259(1)	23.822(1)	12.804(1)	6179(1)
1.3	20.183(1)	23.755(1)	12.778(1)	6127(1)
1.7	20.141(1)	23.704(1)	12.754(1)	6088.4(8)
2.5	20.082(1)	23.613(1)	12.709(1)	6026(1)
2.9	20.038(1)	23.553(1)	12.674(1)	5981.8(9)
3.6	19.949(1)	23.445(2)	12.607(1)	5901(1)
4.1	19.883(1)	23.359(2)	12.572(1)	5839(1)
4.5	19.828(1)	23.29(2)	12.533(1)	5788(1)
5.4	19.736(1)	23.181(1)	12.480(1)	5710(1)
6.1	19.631(1)	23.063(2)	12.422(2)	5624.6(8)
6.6	19.577(2)	22.995(3)	12.392(2)	5579(1)
7.6	19.495(2)	22.903(3)	12.342(2)	5511(2)
5.6(rev)	19.719(2)	23.152(3)	12.473(2)	5694(1)
3.8(rev)	19.967(2)	23.45(3)	12.615(2)	5907(1)
2.4(rev)	20.081(2)	23.621(2)	12.702(1)	6025(1)
P_{amb}(rev)	20.326(3)	23.883(2)	12.836(1)	6231(1)

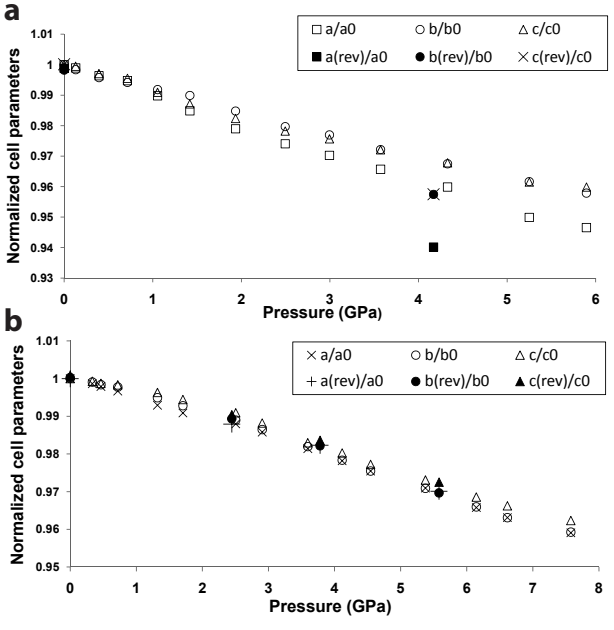

FIGURE 3. Variation of boggsite lattice parameters as a function of pressure. (**a**) Data collected in silicon oil (s.o.); (**b**) data collected in (16:3:1) methanol:ethanol:water (m.e.w). The errors associated with the cell parameters are smaller than the symbol size.

TABLE 4. Details of the structural refinements of boggsite in m.e.w. at selected pressures

	P_{amb}	2.5 GPa	3.6 GPa	P_{amb}(rev)
R_p	5.2	3.3	2.6	2.6
R_{wp}	6.8	2.6	2.1	2.2
$R_{F^{**}2}$	9.4	8.7	8.2	8.8
No. of variables	141	141	141	141
No. of observations	2185	1175	1154	1202

HP-induced structural deformations of boggsite in (16:3:1) methanol:ethanol:water

Framework. The structural deformations induced by HP on boggsite were determined by means of 10 complete Rietveld structural refinements performed from P_{amb} to 3.6 GPa. The results of the refinements corresponding to four selected pressure values [P_{amb}, 2.5 GPa, 3.6 GPa, P_{amb}(rev)] are reported in Tables 5–8 and shown in Figures 4–7. The structural variations induced on the framework up to 3.6 GPa are minimal, consistent with small variations of the unit-cell axes (about 2%) and volume (5%) in this P-range. The decrease of both b and c parameters are due to the flattening of the 4-membered rings surrounding the 12-membered ring channel (Fig. 4). Figure 5 suggests that the c axis contraction also depends on the deformation of the two 6-membered rings above and below the 10-membered ring channel. Considering the uncertainty on the bond distances determined by the structural refinements, neither significant variations in the T-O bond distances nor Si/Al ordering were observed with increasing P (Table 6).

The structural modifications on the channel apertures can be understood by examination of Table 7, which shows the dimensions of the boggsite channels [assuming a spherical shape with radius of 1.35 Å (Shannon 1976) for the framework O atoms] and the Crystallographic Free Area (CFA, sensu Baerlocher et al. 2001) of both channel apertures. According to Pluth and Smith (1990), the 12-membered ring dimensions can be defined by the O15-O15 and O1-O6 distances; the resulting aperture in the sample of this study at P_{amb} is 7.99×7.02 Å. The cross-section of the 10-membered ring channel can be defined using the O8-O8 distance and the average of O9-O9 and O4-O4 distances; dimensions of 5.22×4.80 Å were obtained at P_{amb}. The apparent trends in Table 7 are not regular, however both channel apertures tend to become more circular from P_{amb} to 3.6 GPa.

Extraframework sites. At P_{amb}, 13 extraframework sites were located, in agreement with the results of Zanardi et al. (2004) (Table 5). Most of these sites are far from the framework O atoms (Table 8). For reasons explained below, three of the sites (X1, X7, and X9 in Tables 5 and 8) were tentatively refined with the Ca scattering curve, whereas all the other sites were refined with the oxygen scattering curve. Table 8 shows that several X-X bond distances are too short. Some are acceptable on the basis of the sum (lower than 1) of the occupancy factors of the involved sites (using the scattering curve of oxygen) and are, hence, mutually exclusive. For others, the sum is greater than 1, and hence, these sites are assumed to be occupied by both Ca and water molecules. The refinement allocated 955 electrons, compared to 983 electrons derived from the chemical compositions of boggsite from Antarctica (Table 1).

Upon compression, the occupancy factor increased significantly in extraframework sites X3, X4, X5, X11, and X12. The

TABLE 5. Refined atomic positions and displacement parameters (Å^2) of boggsite in (16:3:1) methanol:ethanol:water at selected pressures

	x/a	*y/b*	*z/c*	Occ.	U_{iso}	*x/a*	*y/b*	*z/c*	Occ.	U_{iso}
			P_{amb}					**2.5 GPa**		
Si1	0.1889(8)	0.1870(5)	0.670(1)	1	0.0163(9)	0.1907(9)	0.1862(8)	0.6680(1)	1	0.015(2)
Si2	0.1873(7)	0.0257(5)	0.329(1)	1	0.0163(9)	0.1855(9)	0.0256(8)	0.322(1)	1	0.015(2)
Si3	0.0751(7)	0.1839(5)	0.833(1)	1	0.0163(9)	0.0781(8)	0.1860(8)	0.833(1)	1	0.015(2)
Si4	0.0772(7)	0.0175(6)	0.165(1)	1	0.0163(9)	0.078(1)	0.0198(9)	0.164(1)	1	0.015(2)
Si5	0.2226(6)	0.0819(6)	0.541(1)	1	0.0163(9)	0.2217(9)	0.0784(8)	0.543(2)	1	0.015(2)
Si6	0.1231(6)	0.0848(6)	0.967(1)	1	0.0163(9)	0.1259(8)	0.0843(9)	0.963(1)	1	0.015(2)
O1	0.195(2)	0.25	0.614(2)	1	0.023(2)	0.180(3)	0.25	0.614(3)	1	0.027(3)
O2	0.120(1)	0.173(1)	0.733(1)	1	0.023(2)	0.123(2)	0.168(1)	0.729(2)	1	0.027(3)
O3	0.199(1)	0.146(9)	0.566(1)	1	0.023(2)	0.201(2)	0.144(1)	0.569(2)	1	0.027(3)
O4	0.183(1)	0.072(1)	0.423(2)	1	0.023(2)	0.201(2)	0.068(1)	0.418(2)	1	0.027(3)
O5	0.115(1)	0.035(1)	0.274(2)	1	0.023(2)	0.110(1)	0.037(1)	0.274(2)	1	0.027(3)
O6	0.092(2)	0.25	0.872(3)	1	0.023(2)	0.100(1)	0.25	0.857(4)	1	0.027(3)
O7	0.00	0.175(2)	0.794(2)	1	0.023(2)	0.00	0.173(2)	0.833(4)	1	0.027(3)
O8	0.00	0.027(2)	0.196(3)	1	0.023(2)	0.00	0.029(2)	0.197(4)	1	0.027(3)
O9	0.186(1)	0.0391(9)	0.619(2)	1	0.023(2)	0.187(2)	0.032(1)	0.614(2)	1	0.027(3)
O10	0.106(1)	0.1515(9)	0.942(1)	1	0.023(2)	0.093(2)	0.146(3)	0.936(2)	1	0.027(3)
O11	0.086(1)	0.074(1)	0.085(2)	1	0.023(2)	0.080(1)	0.065(1)	0.063(2)	1	0.027(3)
O12	0.199(1)	0.0732(9)	0.967(1)	1	0.023(2)	0.203(1)	0.085(1)	0.976(2)	1	0.027(3)
O13	0.099(1)	0.037(1)	0.881(2)	1	0.023(2)	0.103(2)	0.044(1)	0.866(3)	1	0.027(3)
O14	0.25	0.173(2)	0.75	1	0.023(2)	0.25	0.183(3)	0.75	1	0.027(3)
O15	0.25	–0.027(2)	0.75	1	0.023(2)	0.25	–0.023(3)	0.75	1	0.027(3)
X1	0.00	0.178(1)	0.132(2)	0.48(1)	0.154(6)	0.00	0.186(2)	0.172(5)	0.51(2)	0.164(7)
X2	0.181(1)	0.1653(7)	0.235(1)	1.29(2)	0.154(6)	0.164(2)	0.157(1)	0.206(3)	1.30(2)	0.164(7)
X3	0.204(4)	0.25	0.090(5)	0.56(3)	0.154(6)	0.229(4)	0.25	0.058(7)	0.87(4)	0.164(7)
X4	0.099(2)	0.183(1)	0.463(3)	0.65(2)	0.154(6)	0.092(5)	0.136(3)	0.421(9)	0.70(5)	0.164(7)
X5	0.00	0.25	0.555(4)	0.81(4)	0.154(6)	0.00	0.25	0.577(4)	1.65(6)	0.164(7)
X6	0.00	–0.043(1)	0.417(2)	1.11(3)	0.154(6)	0.00	–0.040(2)	0.449(5)	1.19(5)	0.164(7)
X7	0.063(1)	0.153(1)	0.376(2)	0.40(9)	0.154(6)	0.089(4)	0.171(2)	0.417(6)	0.40(2)	0.164(7)
X8	0.035(1)	0.135(1)	0.585(2)	0.72(2)	0.154(6)	0.044(2)	0.110(2)	0.621(4)	0.77(3)	0.164(7)
X9	0.062(2)	0.25	0.286(2)	0.46(1)	0.154(6)	0.046(4)	0.25	0.291(4)	0.42(2)	0.164(7)
X10	0.125(2)	0.25	0.070(3)	1.07(3)	0.154(6)	0.117(4)	0.25	0.061(6)	0.99(4)	0.164(7)
X11	0.202(3)	0.25	0.369(4)	0.73(3)	0.154(6)	0.193(5)	0.25	0.340(7)	0.97(4)	0.164(7)
X12	0.219(5)	0.25	0.243(9)	0.45(3)	0.154(6)	0.190(6)	0.25	0.213(7)	0.81(5)	0.164(7)
X13	0.00	0.060(1)	0.408(3)	0.98(3)	0.154(6)	0.00	0.088(3)	0.352(5)	0.91(4)	0.164(7)
			3.6 GPa					**P_{amb}(rev)**		
Si1	0.1891(8)	0.1880(7)	0.679(1)	1	0.015(2)	0.1889(8)	0.1853(6)	0.669(1)	1	0.015(1)
Si2	0.1883(9)	0.0230(7)	0.318(1)	1	0.015(2)	0.1852(8)	0.0209(8)	0.324(1)	1	0.015(1)
Si3	0.0788(8)	0.1821(6)	0.838(2)	1	0.015(2)	0.0774(8)	0.1854(7)	0.834(1)	1	0.015(1)
Si4	0.0802(6)	0.0183(8)	0.165(2)	1	0.015(2)	0.0780(8)	0.0236(9)	0.167(1)	1	0.015(1)
Si5	0.2179(8)	0.0783(8)	0.542(1)	1	0.015(2)	0.2237(8)	0.0796(7)	0.532(2)	1	0.015(1)
Si6	0.1260(8)	0.0818(9)	0.965(1)	1	0.015(2)	0.1211(8)	0.0826(8)	0.960(1)	1	0.015(1)
O1	0.187(3)	0.25	0.613(3)	1	0.051(3)	0.185(3)	0.25	0.628(3)	1	0.012(3)
O2	0.118(3)	0.173(1)	0.726(2)	1	0.051(3)	0.117(2)	0.173(1)	0.727(2)	1	0.012(3)
O3	0.209(2)	0.145(1)	0.573(2)	1	0.051(3)	0.202(2)	0.141(1)	0.576(2)	1	0.012(3)
O4	0.204(2)	0.067(1)	0.417(2)	1	0.051(3)	0.189(2)	0.071(1)	0.415(2)	1	0.012(3)
O5	0.112(1)	0.040(1)	0.277(2)	1	0.051(3)	0.114(1)	0.044(1)	0.275(2)	1	0.012(3)
O6	0.092(2)	0.25	0.858(4)	1	0.051(3)	0.084(2)	0.25	0.867(3)	1	0.012(3)
O7	0	0.172(2)	0.812(4)	1	0.051(3)	0.00	0.173(2)	0.801(3)	1	0.012(3)
O8	0	0.027(2)	0.172(4)	1	0.051(3)	0.00	0.028(2)	0.196(3)	1	0.012(3)
O9	0.175(1)	0.037(9)	0.617(2)	1	0.051(3)	0.191(2)	0.0404(9)	0.618(2)	1	0.012(3)
O10	0.093(2)	0.142(1)	0.942(2)	1	0.051(3)	0.098(1)	0.1450(11)	0.931(2)	1	0.012(3)
O11	0.088(2)	0.071(1)	0.078(2)	1	0.051(3)	0.092(2)	0.0678(11)	0.074(2)	1	0.012(3)
O12	0.204(8)	0.073(1)	0.974(2)	1	0.051(3)	0.1988(9)	0.0812(11)	0.968(2)	1	0.012(3)
O13	0.106(1)	0.046(9)	0.863(2)	1	0.051(3)	0.103(1)	0.0375(11)	0.874(2)	1	0.012(3)
O14	0.25	0.1927(23)	0.75	1	0.051(3)	0.25	0.185(2)	0.75	1	0.012(3)
O15	0.25	–0.0462(19)	0.75	1	0.051(3)	0.25	–0.0266(19)	0.75	1	0.012(3)
X1	0	0.198(2)	0.119(4)	0.51(1)	0.165(7)	0.00	0.180(2)	0.144(4)	0.53(1)	0.174(8)
X2	0.173(2)	0.157(1)	0.195(3)	1.16(2)	0.165(7)	0.186(2)	0.164(1)	0.221(2)	1.15(2)	0.174(8)
X3	0.306(5)	0.25	0.115(4)	0.88(4)	0.165(7)	0.198(7)	0.25	0.077(7)	0.59(4)	0.174(8)
X4	0.098(2)	0.155(3)	0.315(4)	0.77(3)	0.165(7)	0.130(3)	0.177(3)	0.495(7)	0.53(2)	0.174(8)
X5	0	0.25	0.559(4)	1.61(6)	0.165(7)	0.00	0.25	0.520(7)	0.96(4)	0.174(8)
X6	0	–0.042(2)	0.441(5)	1.19(5)	0.165(7)	0.00	–0.044(2)	0.409(3)	1.11(3)	0.174(8)
X7	0.079(2)	0.163(2)	0.443(3)	0.37(1)	0.165(7)	0.079(1)	0.142(1)	0.379(3)	0.44(1)	0.174(8)
X8	0.0504(18)	0.111(1)	0.605(3)	0.85(3)	0.165(7)	0.050(2)	0.141(2)	0.577(3)	0.71(2)	0.174(8)
X9	0.012(5)	0.25	0.319(4)	0.45(1)	0.165(7)	0.064(3)	0.25	0.294(4)	0.41(1)	0.174(8)
X10	0.175(2)	0.25	0.006(3)	1.19(4)	0.165(7)	0.107(4)	0.25	0.075(5)	0.91(3)	0.174(8)
X11	0.123(4)	0.25	0.232(6)	1.01(5)	0.165(7)	0.179(4)	0.25	0.351(5)	0.96(3)	0.174(8)
X12	0.222(4)	0.25	0.157(5)	0.86(5)	0.165(7)	0.218(9)	0.25	0.157(11)	0.44(5)	0.174(8)
X13	0	0.057(3)	0.359(5)	0.90(4)	0.165(7)	0.00	0.079(4)	0.407(5)	0.90(3)	0.174(8)

Note: Ca scattering curve was chosen for X1, X7, and X9 sites; all the other sites were refined as O atoms.

TABLE 6. T-O framework distances (Å) for boggsite in (16:3:1) methanol:ethanol:water at selected pressures

	P_{amb}	2.5 GPa	3.6 GPa	P_{amb}(rev)
Si1-O1	1.67(1)	1.67(2)	1.618(9)	1.64(2)
-O2	1.65(2)	1.62(2)	1.627(9)	1.63(2)
-O3	1.67(2)	1.62(2)	1.641(9)	1.62(1)
-O14	1.64(1)	1.58(1)	1.584(8)	1.62(1)
mean	1.66	1.62	1.618	1.63
Si2-O4	1.63(2)	1.65(2)	1.655(9)	1.67(2)
-O5	1.64(2)	1.65(2)	1.647(9)	1.67(2)
-O9	1.68(2)	1.59(2)	1.642(9)	1.65(2)
-O15	1.63(1)	1.59(1)	1.597(9)	1.63(1)
mean	1.65	1.60	1.635	1.66
Si3-O2	1.59(2)	1.65(2)	1.633(9)	1.63(2)
-O6	1.69(2)	1.61(2)	1.634(9)	1.61(1)
-O7	1.62(1)	1.60(1)	1.625(9)	1.65(1)
-O10	1.71(2)	1.65(2)	1.630(9)	1.63(2)
mean	1.65	1.63	1.630	1.63
Si4-O5	1.65(2)	1.60(2)	1.626(9)	1.64(2)
-O8	1.63(1)	1.65(2)	1.614(9)	1.63(1)
-O11	1.70(2)	1.66(2)	1.659(9)	1.62(2)
-O13	1.51(2)	1.62(2)	1.627(9)	1.63(1)
mean	1.62	1.63	1.632	1.63
Si5-O3	1.63(2)	1.63(2)	1.612(9)	1.64(2)
-O4	1.74(2)	1.62(2)	1.632(9)	1.67(2)
-O9	1.61(2)	1.57(2)	1.605(9)	1.59(2)
-O12	1.62(2)	1.54(2)	1.574(9)	1.57(1)
mean	1.65	1.59	1.606	1.62
Si6-O10	1.66(2)	1.63(2)	1.592(9)	1.61(2)
-O11	1.71(2)	1.63(2)	1.631(9)	1.62(2)
-O12	1.56(2)	1.55(2)	1.578(9)	1.58(1)
-O13	1.65(2)	1.63(2)	1.600(9)	1.58(2)
mean	1.65	1.61	1.600	1.60

TABLE 7. Selected distances (Å) and areas (Å^2) across 12- and 10-membered ring channels of boggsite in (16:3:1) methanol:ethanol:water at different pressures

P (GPa)	12 MR*	C.F.A.‡	O15-O15	O1-O6	O4-O11	O3-O10
P_{amb}	7.99 × 7.02	40.89	7.99	7.02	6.99	6.86
0.3	7.64 × 7.05	40.91	7.64	7.05	7.00	7.18
0.5	7.87 × 7.23	42.37	7.87	7.23	7.30	7.35
0.7	8.03 × 7.20	42.60	8.03	7.20	7.12	7.11
1.3	8.09 × 7.29	43.10	8.09	7.29	7.15	7.10
1.7	7.54 × 7.33	41.60	7.54	7.33	7.22	7.02
2.5	7.79 × 7.07	41.97	7.79	7.07	7.40	6.98
2.9	7.51 × 7.09	40.43	7.51	7.09	7.11	6.99
3.6	6.76 × 7.11	39.01	6.76	7.11	7.23	7.09
P_{amb}(rev)	7.97 × 7.28	43.19	7.97	7.28	7.16	7.26
P (GPa)	10 MR†	C.F.A.‡	O9-O9	O4-O4	O5-O5	O8-O8
P_{amb}	5.22 × 4.80	19.12	4.84	4.75	4.93	5.22
0.3	5.26 × 4.95	19.90	5.01	4.89	4.98	5.26
0.5	5.27 × 4.89	19.23	4.96	4.81	4.76	5.27
0.7	5.10 × 5.11	20.26	5.24	4.97	5.01	5.10
1.3	5.57 × 5.08	20.76	4.65	5.50	4.85	5.57
1.7	4.99 × 5.02	19.66	4.96	5.08	4.99	4.99
2.5	5.15 × 5.25	20.50	4.81	5.68	4.80	5.15
2.9	5.13 × 4.63	19.76	4.36	4.90	5.68	5.13
3.6	5.03 × 4.87	19.06	4.43	5.30	4.95	5.03
P_{amb}(rev)	5.21 × 5.04	20.20	5.08	5.00	5.00	5.21

* O15-O15 × O1-O6.
† O8-O8 × average of O9-O9 and O4-O4.
‡ Crystallographic Free Area of the channel apertures (sensu Baerlocher et al. 2001) calculated using, for the diameter of the ring, the average of the O-O distances reported in the table.

increase has been reasonably ascribed to the penetration of extra water molecules in these positions. This over-hydration phenomenon can be seen in Figure 6, which shows an increase in the total electron number of extraframework sites as a function of pressure. One can argue that water penetration starts at 0.3 GPa and ceases around 3 GPa. Calculations (total electron number derived by the refinements minus the electrons corresponding to the cation content in the chemical analysis) reveal that 13 extra

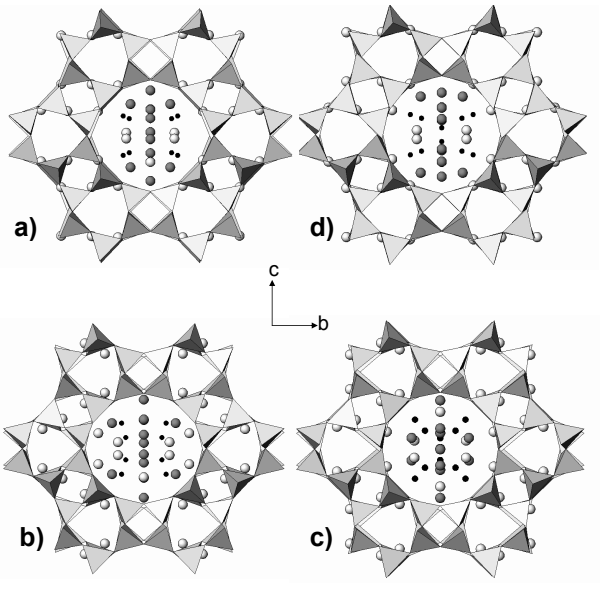

FIGURE 4. Projection of the boggsite structure along [100] at (**a**) P_{amb}, (**b**) 2.5 GPa, (**c**) 3.6 GPa, and (**d**) P_{amb}(rev). Small black circles: X1, X7, X9; large gray circles: X3, X4, X5, X11 X12; large white circles: X2, X6, X8, X10, X13.

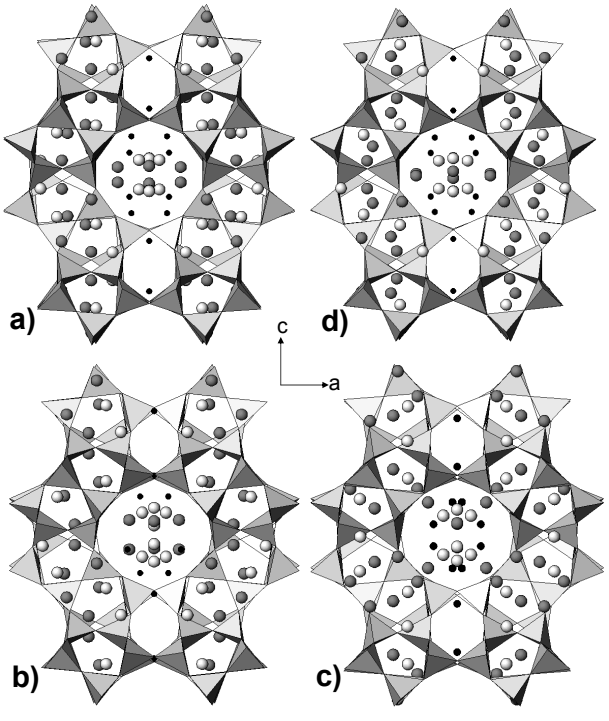

FIGURE 5. Projection of the boggsite structure along [010] at (**a**) P_{amb}, (**b**) 2.5 GPa, (**c**) 3.6 GPa, and (**d**) P_{amb}(rev). Small black circles: X1, X7, X9; large gray circles: X3, X4, X5, X11 X12; large white circles: X2, X6, X8, X10, X13.

TABLE 8. Interatomic distances (<3.20 Å) of the extraframework population for selected refinements of boggsite in (16:3:1) methanol:ethanol:water

	P_{amb}	2.5 GPa	3.6 GPa	P_{amb}(rev)
X1-O11	3.10(2) ×2			
-X1		3.03(11)	2.45(8)	
-X9	2.90(4) ×2	2.33(6) ×2	2.82(6) ×2	2.86(6) ×2
-X10	3.17(3) ×2	3.14(7) ×2		2.87(6) ×2
-X11		3.09(7) ×2	3.14(3)	
X2-O5			3.16(4)	
-O11			2.98(3)	
-O15			3.17(3)	
-X2	2.83(5)			2.70(9)
-X3	2.79(5)	3.17(7)		2.77(7)
-X7	3.01(3)	3.09(8)		3.02(5)
-X10	3.14(3)	3.02(6)		
-X11	2.68(4)	2.84(6)	2.42(5)	2.64(5)
-X12	2.17(4)	2.26(4)	2.44(4)	2.30(8)
-X12	2.88(7)			
-X4		3.13(11)	2.13(4)	
X3-O1		2.86(9)	2.90(5)	
-X2	2.79(5) ×2	3.17(7) ×2		2.77(7) ×2
-X7			3.15(7) ×2	
-X10	1.63(9)	2.24(10)	2.95(9)	1.86(16)
-X11	1.97(10)	2.03(10)	2.39(8)	2.67(17)
-X12	1.99(11)	2.12(10)	1.76(9)	1.11(17)
-X12	2.65(13)		2.93(7)	
X4-O1	3.18(4)			2.70(7)
-O2				2.95(9)
-O3	2.59(4)	2.89(11)		2.04(7)
-O4	3.20(3)	2.86(9)		3.00(7)
-O5		3.01(9)	2.75(6)	
-X2			2.13(4)	
-X4	3.19(7)	3.13(11)		
-X5	2.83(5)			
-X7	1.51(4)	0.82(10)	1.67(7)	2.00(8)
-X8	2.33(5)	2.79(10)		2.12(8)
-X9	2.87(4)		2.82(8)	
-X11	2.90(6)		2.51(6)	2.72(10)
-X13		2.35(12)	3.05(7)	
X5-X4	2.83(5) ×4			3.18(6) ×4
-X8	2.85(3) ×4			2.90(4) ×4
-X7			2.96(5) ×4	
-X9			3.04(6) ×2	3.18(8) ×2
X6-O8				3.11(5)
-X6	2.95(6)	2.30(8)	2.47(8)	3.13(8)
-X8	2.33(4) ×2	2.08(5) ×2	1.99(4) ×2	2.54(6) ×2
-X13	2.45(4)	2.77(8)	2.56(9)	2.93(7)
-X13	2.28(4)		2.55(6)	2.50(7)
X7-O3		3.03(8)	3.00(4)	
-O4	3.17(2)			2.84(3)
-O5				2.86(4)
-X2	3.01(3)	3.09(8)		3.02(5)
-X3			3.15(7)	
-X4	1.51(4)	0.82(10)	1.67(7)	2.00(8)
-X5			2.96(5)	
-X7	2.57(4)		3.15(8)	
-X8	2.77(4)	3.10(8)	2.45(4)	2.61(5)
-X9	2.58(3)	2.62(7)	2.90(7)	2.82(4)
-X11		2.97(9)		
-X13	2.61(4)	2.79(8)	3.12(8)	2.23(6)
X8-O2	2.72(3)	2.50(5)	2.49(4)	2.45(5)
-O3			3.18(4)	3.15(4)
-O7	2.93(2)			
-X4	2.33(5)	2.79(10)		2.12(8)
-X5	2.85(3)			2.90(4)
-X6	2.33(4)	2.08(5)	1.99(4)	2.54(6)
-X7	2.77(4)	3.10(8)	2.45(4)	2.61(5)
-X8	1.43(6)	1.78(9)	2.01(7)	2.06(8)
-X13	2.99(4)			2.83(8)
X9-X1	2.90(4) ×2	2.33(6) ×2	2.82(6) ×2	2.86(6) ×2
-X4	2.87(4) ×2		2.82(8) ×2	
-X5			3.04(6)	
-X7	2.58(3) ×2	2.62(7) ×2	2.90(7) ×2	2.82(4) ×2
-X7			3.14(7) ×2	
-X9	2.52(7)	1.84(14)	0.47(2)	2.62(11)
-X10	3.05(5)			2.93(8)
-X11	3.05(7)	3.03(11)	2.47(11)	2.44(8)
-X11			2.90(11)	
-X12		3.06(16)		
X10-O6	2.63(3)	2.62(8)	2.51(5)	2.73(6)
-O10	2.90(2) ×2	2.97(4) ×2	3.11(3)	3.07(4) ×2
-X1	3.17(3) ×2	3.14(7) ×2		2.87(6)
-X2	3.14(3) ×2	3.02(6) ×2		
-X3	1.63(9)	2.24(10)	2.95(9)	1.86(16)
-X9	3.05(5)			2.93(8)
-X12	2.93(11)	2.43(10)	2.12(6)	2.50(16)
X11-O1	3.16(5)			
-X1			3.09(7) ×2	
-X2	2.68(4) ×2	2.84(6) ×2	2.45(5)	2.64(5) ×2
-X3	1.97(10)	2.03(10)	2.39(8)	2.67(17)
-X4	2.90(6) ×2		2.51(6) ×2	2.72(10) ×2
-X7		2.97(9) ×2		
-X9	3.05(7)	3.03(11)	2.47(11)	2.44(8)
-X9			2.90(12)	
-X12	1.65(11)	1.61(7)	2.19(9)	2.61(14)
-X12	2.14(12)	2.43(12)		2.09(17)
X12-X2	2.17(4) ×2	2.26(4) ×2	2.44(4) ×2	2.30(8) ×2
-X2	2.88(7) ×2		2.96(7)	
-X3	1.99(11)	2.12(10)	1.76(9)	1.11(17)
-X3	2.65(13)			
-X9		3.06(16)		
-X10	2.93(11)	2.43(10)	2.12(6)	2.50(16)
-X11	1.65(11)	1.61(7)	2.19(9)	2.61(14)
-X11	2.14(12)	2.43(12)		2.09(17)
-X12	1.26(20)	2.57(23)	2.60(1)	2.71(27)
X13-O5	2.96(3) ×2	2.70(4) ×2	2.49(3) ×2	3.03(5) ×2
-O8	2.83(4)	2.40(7)	2.46(6)	2.99(8)
-X4		2.35(12) ×2	3.05(7) ×2	
-X6	2.45(4)	2.77(8)	2.56(9)	2.93(7)
-X6	2.28(4)	2.79(8) ×2	2.55(6)	2.50(7)
-X7	2.61(4) ×2		3.12(8) ×2	2.23(6) ×2
-X8	2.99(4) ×2			2.83(8) ×2

water molecules penetrate boggsite structure in this *P* range. This corresponds to an increase of about 14% of the total water content of the zeolite.

Most extraframework sites are statistically occupied by both Ca and water molecules. Three of the sites (X1, X7, and X9 in Tables 5 and 8) were tentatively refined with the Ca scattering curve based on a combination of the following assumptions: (1) occupancy in these sites does not increase significantly upon compression, suggesting that no extra water molecules enter into these positions, and (2) the X-X bond distances in the sites are reasonable following the first assumption. However, these three sites likely also host some water molecules because, otherwise, the number of electrons in these crystallographic positions would be greater than that obtained for the cations from the chemical analysis (Table 1).

Reversibility. Figure 3 and Table 3 illustrate the reversibility of the HP-induced unit-cell parameters in boggiste when compressed in m.e.w. Furthermore, the original water content is restored upon pressure release. However, the framework structural deformations are not completely reversible (Table 7). Upon decompression, the 12-membered ring channel becomes much larger and more circular than that at ambient conditions and its CFA is similar to that observed at 1.3 GPa, and the larger CFA of the 10-membered ring channel does not completely

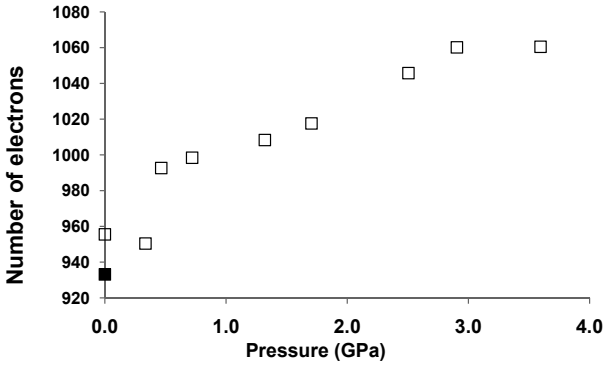

FIGURE 6. Total number of electrons in the extraframework sites as a function of pressure for boggsite compressed in (16:3:1) methanol:ethanol:water; black square represents the total extra framework electrons at P_{amb} after decompression.

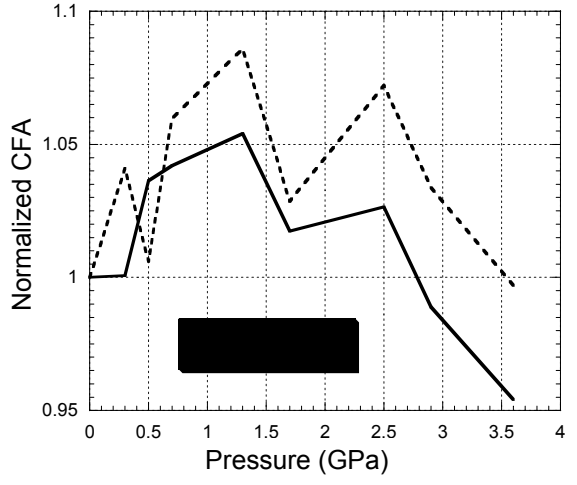

FIGURE 7. Evolution of the 10- and 12-membered rings normalized to CFA as a function of pressure.

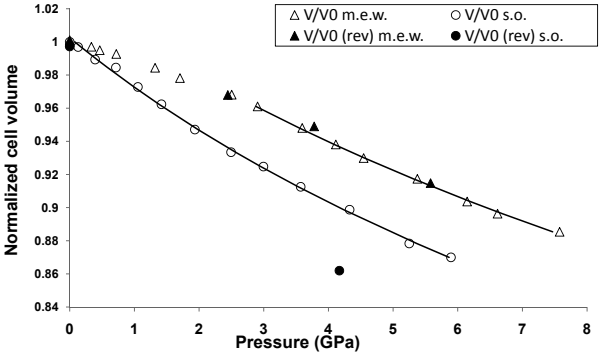

FIGURE 8. Comparison of the unit-cell volume as a function of pressure for boggsite compressed in silicon oil (circles) and (16:3:1) methanol:ethanol:water (triangles). The lines represent the fits obtained using second-order Birch-Murnaghan equations of state.

regain the original value. These data suggest that the water loss accompanying pressure release requires pore openings as suggested by zeolite dehydration studies, which indicate that water molecules migrate out of the cavities (see, i.e., Cruciani and Gualtieri 1999).

During compression, all extraframework sites undergo a significant re-organization (Figs. 4 and 5). However, the new site distribution is not completely reversible (positions of the extraframework sites present in boggsite at P_{amb} are not quite regained). This is particularly evident in the projection along [010] (Fig. 5).

CONCLUDING REMARKS

It is worth noting that over-hydration of boggsite occurs without any cell-volume expansion, similarly to that found for over-hydrated gismondine (Ori et al. 2008). In both phases, no new extraframework sites arise during the over-hydration process and water penetration only effects an increase in the occupancy factor of already existing sites. An interesting difference between boggsite and in gismondine over-hydration is the reversibility of the process; in gismondine, the penetrated water molecules remain in the pores (Ori et al. 2008), whereas boggsite releases the extra water molecules upon decompression.

Figure 7 illustrates the normalized CFA as a function of pressure for both channels. The trends are similar, with some irregularities, and show an increase in channel aperture area during water penetration. As expected, above 2.5 GPa, subsequent to stabilization of water content (Fig. 6), a compression of the pores is observed.

It is interesting to compare the elastic behavior of boggsite compressed in m.e.w. and in s.o. In both cases, no complete amorphization is observed (Figs. 2b–2c) and the unit-cell parameters of P_{amb} are recovered upon decompression (Fig. 3), even though a large hysteresis effect is observed in s.o. Figure 8 shows that boggsite compressibility is higher in s.o. than in m.e.w. Moreover, compressibility in m.e.w. is lower below 3 GPa, whereas above this pressure, the *P-V* trend becomes similar in the two media. This is due to the fact that during the water molecule penetration ($0.3 < P < 3$ GPa) the effect of the *P*-transmitting medium is not only directed to compress the structure, but also to penetrate the channels. Subsequent to over-hydration phenomenon (around 3 GPa), boggsite compressibility in m.e.w. increases and becomes similar to that observed in s.o.

Boggsite is highly compressible (K_0 = 31 and 37 GPa in s.o. and m.e.w., respectively), when compared to other zeolites studied under HP conditions. On the contrary, boggsite structure is extremely rigid during dehydration, accompanied by volume contraction less than 1.4% (up to 500 °C) (Zanardi et al. 2004). This behavior has also been observed for zeolite A (Pluth and Smith 1980; Arletti et al. 2003) and bikitaite (Ferro et al. 2002) and is the reverse of that observed in gismondine (Vezzalini et al. 1993; Ori et al. 2008).

ACKNOWLEDGMENTS

The Swiss-Norwegian (BM01) and GILDA (BM08) beamlines at European Synchrotron Radiation Facility are acknowledged for allocation of the experimental beamtime. The authors are indebted to Ermanno Galli for providing polycrystalline boggsite material from the Antarctica rock samples, and to Vladimir Dmitriev for technical support during the HP experiments. Two anonymous reviewers are

acknowledged for the useful comments that contributed to improving the quality of the paper.

REFERENCES CITED

Alberti, A. and Martucci, A. (2005) Studies in surface science and catalysis. In A. Gamba, C. Colella, and S. Coluccia, Eds., Oxide Based Materials: New Sources, Novel Phases, New Applications, p. 19–43. Elsevier, Amsterdam.

Alberti, A., Cruciani, G., Galli, E., Merlino, S., Millini, R., Quartieri, S., Vezzalini, G., and Zanardi, S. (2001) Pentasil zeolites from Antartica: From mineralogy to zeolite sciences and technology. In A. Galarneau, F. Di Renzo, F. Famula, and J. Vedrine, Eds., Studies in Surface Science and Catalysis, 135, p. 83–91. Elsevier, Amsterdam.

Angel, R.J. (2001) EOS-FIT V5.2. Computer program. Crystallography Laboratory, Department of Geological Sciences, Virginia Tech, Blacksburg, Virginia.

Arletti, R., Ferro, O., Quartieri, S., Sani, A., Tabacchi, G., and Vezzalini, G. (2003) Structural deformation mechanisms of zeolites under pressure. American Mineralogist, 88, 1416–1422.

Baerlocher, Ch., Meier, W.M., and Olson, D.H. (2001) Atlas of Zeolite Framework Types, 5th revised edition. Elsevier, Amsterdam.

Birch, F. (1974) Finite elastic strain of cubic crystal. Physical Review, 71, 809–824.

Bish, D.L. and Carey, J.W. (2001) Thermal behavior of natural zeolites. In D.L. Bish and D.W. Ming, Eds., Natural Zeolites: Occurrence, properties, applications, 45, p. 403–452. Reviews in Mineralogy and Geochemistry, Mineralogical Society of America, Chantilly, Virginia.

ChePa, F. and Baharun, N. (2005) Hydrothermal synthesis of zeolites from Sultan Salahuddin Abdul Aziz Shah power plant fly ash. Journal of Physical Science, 16, 111–120.

Clark, L.A., Ye, G.T., and Snurr, R.Q. (2000) Molecular traffic control in a nanoscale system. Physical Review Letters, 84, 2893–2896.

Corma, A. (1997) From microporous to mesoporous molecular sieve materials and their use in catalysis. Chemical Review, 97, 2373–2420.

Cruciani, G. (2006) Zeolites upon heating: Factors governing their thermal stability and structural changes. Journal of Physics and Chemistry of Solids, 67, 1973–1994.

Cruciani, G. and Gualtieri, A. (1999) Dehydration dynamics of analcime by in situ synchrotron powder diffraction. American Mineralogist, 84, 112–119.

Ferro, O., Quartieri, S., Vezzalini, G., Fois, E., Gamba, A., and Tabacchi, G. (2002) High-pressure behavior of bikitaite: An integrated theoretical and experimental approach. American Mineralogist, 87, 1415–1425.

Fois, E., Gamba, A., Tabacchi, G., Arletti, R., Quartieri, S., and Vezzalini, G. (2004) The template effect of the extra-framework content on zeolite compression: The case of yugawaralite. American Mineralogist, 90, 28–35.

Fois, E., Gamba, A., Medici, C., Tabacchi, G., Quartieri, S., Mazzucato, E., Arletti, R., Vezzalini, G., and Dmitriev, V. (2008) High pressure deformation mechanism of Li-ABW: Synchrotron XRPD study and ab initio molecular dynamics simulations. Microporous and Mesoporous Materials, 115, 267–280.

Forman, R.A., Piermarini, G.J., Barnett, J.D., and Block, S. (1972) Pressure measurements made by utilization of the ruby sharp-line luminescence. Science, 176, 284–286.

Galli, E., Quartieri, S., Vezzalini, G., and Alberti, A. (1995) Boggsite and tschernichite-type zeolites from Mt. Adamson, Northern Victoria land (Antarctica). European Journal of Mineralogy, 7, 1029–1032.

Gatta, G.D. (2008) Does porous mean soft? On the elastic behaviour and structural evolution of zeolites under pressure. Zeitschrift für Kristallographie, 223, 160–170.

Hammersley, A.P., Svensson, S.O., Hanfland, M., Fitch, A.N., and Häusermann, D. (1996) Two-dimensional detector software: from real detector to idealized image or two-theta scan. High Pressure Research, 14, 235–248.

Howard, D.G., Tschernich, R.W., Smith, J.V., and Klein, G.L. (1990) Boggsite, a new high-silica zeolite from Goble, Columbia County, Oregon. American Mineralogist, 75, 1200–1204.

Larson, A.C. and Von Dreele, R.B. (1996) GSAS, General Structure Analysis System. Report LAUR 86-748, Los Alamos National Laboratory, Los Alamos, New Mexico.

Leardini, L., Quartieri, S., and Vezzalini, G. (2010) Compressibility of microporous materials with CHA topology: 1. Natural chabazite and SAPO-34. Microporous and Mesoporous Materials, 127, 219–227.

Lee, Y., Hriljac, J.A., Studer, A., and Vogt, T. (2004) Anisotropic compression of edingtonite and thomsonite to 6 GPa at room temperature. Physics and Chemistry of Minerals, 31, 22–27.

Mao, H.K., Xu, J., and Bell, P.M. (1986) Calibration of the ruby pressure gauge to 800 kbar under quasi-hydrostatic conditions. Journal of Geophysical Research, 91, 4673–4676.

Miletich, R., Allan, D.R., and Kush, W.F. (2000) High-pressure single-crystal techniques. In R.M. Hazen and R.T. Downs, Eds., High-Temperature and High-Pressure Crystal Chemistry, 41, p. 445–519. Reviews in Mineralogy and Geochemistry, Mineralogical Society of America and Geochemical Society, Chantilly, Virginia.

Ori, S., Quartieri, S., Vezzalini, G., and Dmitriev, V. (2008) Pressure-induced overhydration and water ordering in gismondine: A synchrotron powder diffraction study. American Mineralogist, 93, 1393–1403.

Pluth, J.J. and Smith, J.V. (1980) Accurate redetermination of crystal structure of dehydrated zeolite A. Absence of near zero coordination of sodium. Refinement of Si,Al-ordered superstructure. Journal of American Chemical Society, 102, 4704–4708.

——— (1990) Crystal structure of boggsite, a new high-silica zeolite with the first three-dimensional channel system bounded by both 12- and 10-rings. American Mineralogist, 75, 501–507.

Sanborn, M.J., Gupta, A., Clark, L.A., and Snurr, R.Q. (2001) Molecular modeling of multicomponent diffusion in zeolites and zeolite membranes. In A. Galarneau, F. Di Renzo, F. Famula, and J. Vedrine, Eds., Studies in Surface Science and Catalysis, 135, p. 1–7. Elsevier, Amsterdam.

Shannon, G.M. (1976) Revised effective ionic radii and systematic studies of interatomic distances in halides and chalcogenides. Acta Crystallographica, A32, 751–767.

Thomson, P., Cox, D.E., and Hastings, J.B. (1987) Rietveld refinement of Debye-Scherrer synchrotron X-ray data from Al_2O_3. Journal of Applied Crystallography, 20, 79–83.

Toby, B.H. (2001) EXPGUI, a graphical user interface for GSAS. Journal of Applied Crystallography, 34, 210–213.

Vezzalini, G., Quartieri, S., and Alberti, A. (1993) Structural modifications induced by dehydration in the zeolite gismondine. Zeolites, 13, 34–42.

Zanardi, S., Cruciani, G., Alberti, A., and Galli, E. (2004) Dehydration and rehydration process in boggsite: An in situ X-ray single-crystal study. American Mineralogist, 89, 1033–1042.

MANUSCRIPT RECEIVED DECEMBER 23, 2009
MANUSCRIPT ACCEPTED MAY 2, 2010
MANUSCRIPT HANDLED BY AARON CELESTIAN